Site-Specific Ultra-Low-Sidelobe Phased Array Topologies for Sparse Areas of Particular Shape

Aslan, Yanki

DOI
10.23919/EuMC54642.2022.9924381

Publication date
2022

Document Version
Final published version

Published in
Proceedings of the 52nd European Microwave Conference (EuMC)

Site-Specific Ultra-Low-Sidelobe Phased Array Topologies for Sparse Areas of Particular Shape

Yanki Aslan
Microwave Sensing, Signals and Systems Group, Department of Microelectronics,
Faculty of Electrical Engineering, Mathematics, and Computer Science,
Delft University of Technology, Delft, The Netherlands
Y.Aslan@tudelft.nl

***Abstract* — Optimal design of uniformly-fed aperiodic millimeter-wave phased array topologies for site-specific and quasi interference-free operation is presented. Several use cases with different number of line-of-sight cells in the close vicinity of the base station, and for various widths and shapes of the cells, are analyzed. The arrays are synthesized by applying an iterative convex optimization technique. The simulation results of 256-element arrays indicate strong intra-cell and inter-cell isolation with around -40 dB maximal side lobe level. The proposed technique is found to be especially useful in the application scenarios supporting sparsely distributed narrow communication cells.**

***Keywords* — 5G, antenna radiation patterns, communication systems, optimization methods, phased arrays.**

I. Introduction

The currently proposed regular square-grid [1], [2] or triangular-grid [3], [4] phased array layouts are far from the optimal site-specific array topologies when various deployment scenarios and dynamic traffic needs of the next-generation mm-wave base station antennas are considered. This is due to the statistically large intra-cell and inter-cell interference originating from the high side lobes in multiuser communication with the one-beam-per-user concept which exploits the same time-frequency resources for increased throughput [5]. Applying amplitude and/or phase tapering for side lobe reduction causes significant decrease in the array efficiency and limits flexible re-use of the resources [6], [7].

In contrary to the conventional counterparts, the large-scale aperiodic phased arrays with uniform amplitudes and linear phases have the advantage of suppressing the high side lobes, thus the average interference, while keeping the optimal power efficiency [8]. This will be especially useful when the communication environment owns or supports sparse (by the physical or angular distance) and (angularly) narrow cells, since such array topologies will have the ability to push the high side lobes outside the sectors of interest with enough area and suppress the ones within much further.

In such particular scenarios, two generalized mm-wave use cases can be considered. In the first case, there may be only one cell both in the line-of-sight (LoS) and in the vicinity of the base station. Then, the high side lobes outside the cell will not contribute significantly to the intra-cell or inter-cell interference as (i) they will reach the nearby cell through a non-line-of-sight (NLoS) path with a large loss, and (ii) they will lose their strength when they reach the neighboring LoS cells further away. In the literature, it was pointed out that in mm-wave networks the interference stems from the LoS interferers and the NLoS interference is negligible [9]–[12]. Several studies reported between 25-40 dB reduction in the NLoS signal levels as compared to the LoS [13]–[16]. In the second case, there may be multiple narrow cells in the LoS and closely located to the base station. Then, the side lobes are simultaneously suppressed both within the cell associated to the optimized array and within the neighboring cells.

In this paper, the above-mentioned two generic use cases are analyzed with different cell realizations. In addition, new site-specific array topologies with ultra-low maximal side lobes (at around -40 dB) within the cells are proposed. From the realization point of view, such arrays can be either designed uniquely for the site (or for a number of standardized application-representative sites), or with some compromise in performance and complexity, a generic design can be made with a mechanically [17] or digitally [18] reconfigurable layout. Another appealing option would be to have a single-type oversized array on a fixed grid and apply site/traffic-specific thinning [19], yet this is not compatible with the flexibility offered with the topologies proposed in this paper and will result in strong performance degradation in terms of the side lobes.

The rest of the paper is organized as follows. Section II formulates the optimization method. Section III presents the simulation results. The conclusions are given in Section IV.

II. Array Topology Optimization

We apply the Iterative Convex Optimization (ICO) technique to our original simulation scenarios. The ICO method is based on small progressive position perturbations of the antenna elements which are fed with uniform amplitudes and linear phase shifts [20]. The iterative nature of the algorithm is used to linearize the non-linear array factor expression around the element locations [21]. The topologies synthesized via ICO provide optimal power efficiencies with strong suppression of side lobes for multiple scan angles simultaneously. This section aims to briefly discuss the formulation of the ICO problem within our context.

Consider an N element array on the xy-plane with the indices $n = 1, 2, ..., N$ with a given initial topology (e.g. on

a square, triangular or circular grid). Assume at iteration i, element n is moved by $\epsilon_n^{(i)}$ in the $\hat{\mathrm{x}}$, and $\delta_n^{(i)}$ in the $\hat{\mathrm{y}}$ direction. When the values of these perturbations are restricted to be much smaller than the wavelength at the design frequency and equi-amplitude/linear phase excitations are used, the expression of the (normalized) electric far-field at iteration i in the $u = \sin\theta\cos\phi, v = \sin\theta\sin\phi$ plane coordinates (denoted here as $f^{(i,u_s,v_s)}_{\boldsymbol{\epsilon}^{(i)},\boldsymbol{\delta}^{(i)}}(u,v)$ for a scanned beam s with the maximum at u_s, v_s) can be approximated as [20]

$$f^{(i,u_s,v_s)}_{\boldsymbol{\epsilon}^{(i)},\boldsymbol{\delta}^{(i)}}(u,v) \approx \frac{1}{N}\sum_{n=1}^{N} E_n^{(i)}(u,v) e^{jk(u-u_s x_n^{(i-1)})} e^{jk(v-v_s)y_n^{(i-1)}}(1 + jk(u-u_s)\epsilon_n^{(i)} + jk(v-v_s)\delta_n^{(i)}) \quad (1)$$

where k is equal to $2\pi/\lambda$ for the free-space wavelength at the single design frequency, and $E_n^{(i)}(u,v)$ denotes the embedded element pattern of element n at iteration i. It is worth to note that the formulation can be extended to multiple design frequencies (within a desired band) as in [22], which is out of scope of this paper.

Besides, obtaining the embedded patterns for mutual coupling inclusion requires extra simulation efforts that grow substantially with the increasing number of elements [23]. Efficient computation of embedded patterns in aperiodic array synthesis is an active and open research topic [24]. Thus, currently many researchers consider a minimal element separation, $d_{\min} \geq 0.5\lambda$, and ignore the pattern variations among the elements, which is also the approach followed in this work. To satisfy the constraint on $d_{\min}$ for every element pair (m,n), the following approximation of the Euclidean distance must hold [20]

$$(\epsilon_m^{(i)} - \epsilon_n^{(i)})(2x_m^{(i-1)} - 2x_n^{(i-1)}) + (\delta_m^{(i)} - \delta_n^{(i)})(2y_m^{(i-1)} - 2y_n^{(i-1)}) + (x_m^{(i-1)} - x_n^{(i-1)})^2 + (y_m^{(i-1)} - y_n^{(i-1)})^2 \geq d_{\min}^2 \quad (2)$$

Following (1), the side lobe region for the sector of interest is defined (here denoted as $(\boldsymbol{u},\boldsymbol{v})_{SL}$ containing the proper set of u, v coordinates) by considering the in-sector and (if significant) cross-sector interference for flexible beam scanning at any angular direction within the sector of interest. We also assume a circular main beam shape with the radius r, which can be modified if needed.

In a compact form, the ICO problem at iteration i is formulated as

$$\min_{\boldsymbol{\epsilon}^{(i)},\boldsymbol{\delta}^{(i)}} \rho^{(i)}, \ s.t. \ \begin{cases} |f^{(i,u_s,v_s)}_{\boldsymbol{\epsilon}^{(i)},\boldsymbol{\delta}^{(i)}}((\boldsymbol{u},\boldsymbol{v})_{SL})| \leq \rho^{(i)} \text{ holds } \forall s, \\ |\boldsymbol{\epsilon}^{(i)}| \leq \mu, \ |\boldsymbol{\delta}^{(i)}| \leq \mu, \\ (2) \text{ holds } \forall (m,n) \in \{1,...,N\}, m \neq n \end{cases} \quad (3)$$

where $\boldsymbol{\epsilon}^{(i)} = \begin{bmatrix} \epsilon_1^{(i)} & \cdots & \epsilon_N^{(i)} \end{bmatrix}$ and $\boldsymbol{\delta}^{(i)} = \begin{bmatrix} \delta_1^{(i)} & \cdots & \delta_N^{(i)} \end{bmatrix}$. The maximal side lobe level is represented by the symbol ρ. The upper bound for the position perturbations is denoted by μ, which should be small enough to satisfy the linear approximations and achieve stable convergence of $\rho^{(i)}$.

The optimization problem in (3) is a second order cone programming problem [25]. In this work, it is solved by using the SDPT3 semidefinite programming solver in CVX [26]. Throughout the simulations in the paper, the following settings are used: N = 256, r = 0.1, μ = 0.08λ, $d_{\min} = 0.5\lambda$, $E_n = \sqrt{\cos\theta}$, uv-plane is on a square grid with the steps of 0.02, and initial array layout is 16×16 square with 0.5λ spacing. With these settings, each iteration takes only a few minutes in a 32-processor Intel(R) Xeon(R) CPU E5-2650 v2 @2.60GHz 128GB RAM Red Hat Enterprise Linux Server. The convergence in ρ is achieved within 100 iterations in all the cases studied in the paper.

III. Simulation Results

We focus on five use cases with various cell definitions in two generic groups. In the first group (Case 1-a to c, there is only one relatively narrow cell in the close vicinity and LoS of the base station. We select rather unconventional cell shapes (T-shape, bow tie-shape and star-shape) to reflect the site-specific nature of the problem. In the second group (Case 2-a and b), there are multiple rectangular narrow cells in the close vicinity and LoS-region of the base station. The array communicates with the users only in a single pre-defined cell, while the other neighboring cells have additional arrays dedicated to them. Table 1 provides the short descriptions of the use cases. The optimized array topologies synthesized by using the ICO technique as described in Section II are given in Fig. 1 for each case. The cells corresponding to each scenario and the corresponding regions of interference for side lobe minimization are visualized in the uv-plane in Fig. 2 and Fig. 3 for Case 1 and Case 2, respectively.

The final layouts correspond to the converged level of maximal side lobe level and are plotted after the iteration number 100. In all array layouts, the minimum spacing between the elements is kept at 0.5λ. The overall circular shape of the arrays naturally comes from the definition of the main lobe within a circle. The corresponding values of ρ^i for i = 100 are listed in Table 1. Furthermore, for better visualization, the (normalized) array radiation patterns associated to the optimal array topologies are given in Fig. 4 and Fig. 5 for multiple scan directions in the cells for Case 1 and Case 2, respectively.

Table 1. Description of the use cases studied in the paper and the corresponding maximal side lobe level outcome with the optimized array topology

Use case	Description	$\rho^{(i)}$ (dB), at i = 100
1-a	Single nearby LoS cell, narrow T-shaped	-37.4
1-b	Single nearby LoS cell, narrow bow tie-shaped	-42.0
1-c	Single nearby LoS cell, narrow star-shaped	-42.3
2-a	An off-broadside and a neighboring nearby LoS cells, narrow rectangular-shaped	-41.8
2-b	A broadside and four neighboring nearby LoS cells, narrow rectangular-shaped	-39.6

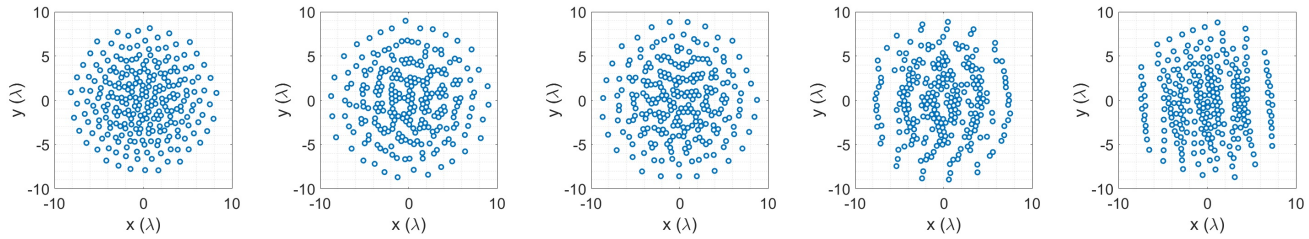

Fig. 1. Optimized array topologies for case: (a) 1-a, (b) 1-b, (c) 1-c, (d) 2-a, (e) 2-b.

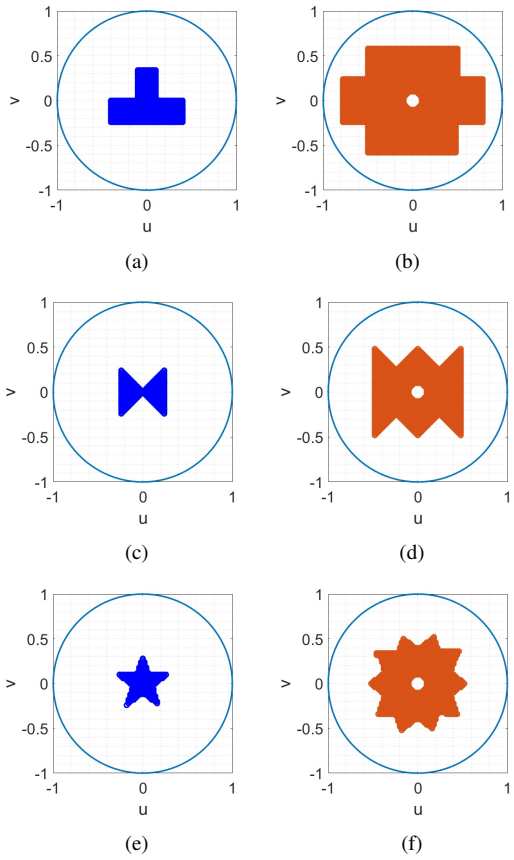

Fig. 2. Single LoS cell definitions and side lobe regions in the uv-plane: (a) case 1-a, cell definition, (b) case 1-a, side lobe region, (c) case 1-b, cell definition, (d) case 1-b, side lobe region, (e) case 1-c, cell definition, (f) case 1-c, side lobe region.

From the simulation results, it can be observed that for the use cases of our interest, the optimized site-specific array topologies strongly reduce the intra-cell and inter-cell interference by providing ultra-low side lobe levels around -40 dB. The level changes by a few dB's depending on the width of the cells, thus the side lobe region, which is expected as this region defines the area to move the high side lobes to improve isolation inside the cells. Besides, as verified in [8], with this approach, the array directivities are kept at optimal levels, which are close or better than the directivity of an equi-amplitude/linear-phase 0.5λ regularly spaced array since there is no amplitude/phase tapering and the cell widths for beam scanning are narrow. Note that for the studied cases the

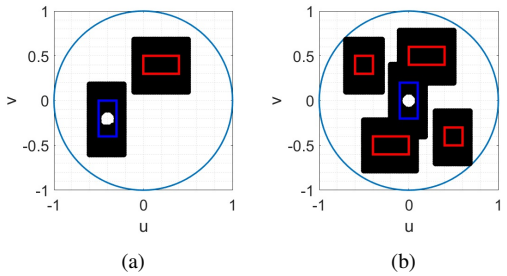

Fig. 3. Multiple LoS cell definitions and side lobe regions in the uv-plane, use case: (a) 2-a, (b) 2-b. Note: Blue rectangle shows the sector-of-interest, red rectangles show the neighboring LoS cells, black region is the corresponding side lobe region.

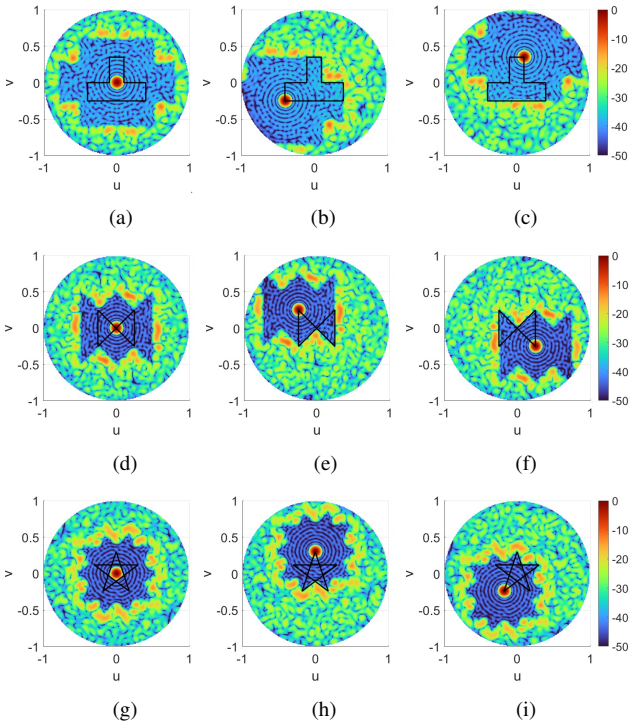

Fig. 4. Array radiation patterns (normalized, in dB) with scanning for the single LoS cells in use case: (a) 1-a, center beam, (b) 1-a, beam at left bottom corner, (c) 1-a, beam at right top corner, (d) 1-b, center beam, (e) 1-b, beam at left top corner, (f) 1-b, beam at right bottom corner, (g) 1-c, center beam, (h) 1-c, beam at upper corner, (i) 1-c, beam at left bottom corner.

maximal side lobe level stays around or higher than -30 dB if the optimization is performed by covering the whole visible space instead of the sectors only.

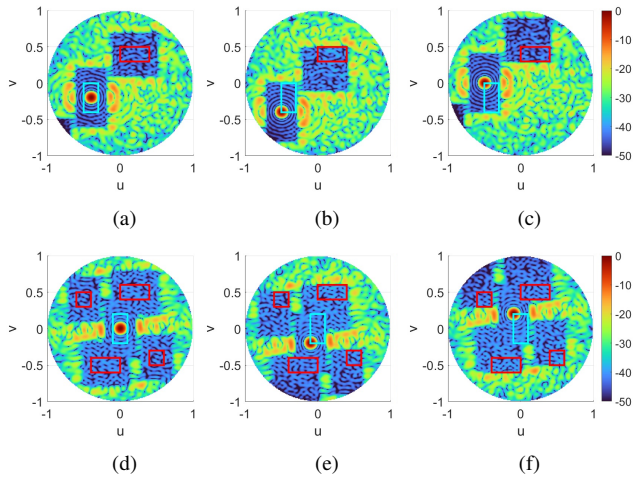

Fig. 5. Array radiation patterns (normalized, in dB) with scanning for multiple nearby LoS cells in use case: (a) 2-a, center beam, (b) 2-a, beam at bottom left corner, (c) 2-a, beam at top left corner, (d) 2-b, center beam, (e) 2-b, beam at bottom left corner, (f) 2-c, beam at top left corner.

IV. Conclusion

The problem of intra- and inter-cell interference accumulation in the LoS-dominant mm-wave networks has been addressed. The study has focused on the scenarios where the proposed technique is the most effective, which is when the environment supports the deployment of relatively sparse (by the distance, number and/or angle) and narrow (by the angle) communication cells. Novel and unique aperiodic, uniform-amplitude/linear-phase fed array topologies have been synthesized for site/traffic specific operation by using an iterative convex optimization algorithm. For demonstration purposes, 256 array elements and cell definitions with various shapes and widths in the angular domain have been used. The isolation within the cells have been significantly improved with around -40 dB maximal side lobe level.

Acknowledgment

The author would to like thank Prof. Alexander Yarovoy from the Delft University of Technology for his valuable comments on the paper.

References

[1] B. Sadhu *et al.*, "A 28 GHz 32-element phased-array transceiver IC with concurrent dual polarized beams and 1.4 degree beam-steering resolution for 5G communication," in *Proc. IEEE ISSCC*, San Francisco, CA, USA, Feb. 2017.

[2] Y. Aslan, C. E. Kiper, A. J. van den Biggelaar, U. Johannsen, and A. Yarovoy, "Passive cooling of mm-wave active integrated 5G base station antennas using CPU heatsinks," in *Proc. 16th EuRAD*, Paris, France, Oct. 2019, pp. 121–124.

[3] F. A. Dicandia and S. Genovesi, "Exploitation of triangular lattice arrays for improved spectral efficiency in massive MIMO 5G systems," *IEEE Access*, vol. 9, pp. 17 530–17 543, 2021.

[4] R. Valkonen, "Compact 28-GHz phased array antenna for 5G access," in *Proc. IEEE/MTT-S IMS*, Philadelphia, Pennsylvania, Jun. 2018.

[5] W. Hong *et al.*, "Multibeam antenna technologies for 5G wireless communications," *IEEE Trans. Antennas Propag.*, vol. 65, no. 12, pp. 6231–6249, Jun. 2017.

[6] Y. Aslan, J. Puskely, A. Roederer, and A. Yarovoy, "Phase-only control of peak sidelobe level and pattern nulls using iterative phase perturbations," *IEEE Antennas Wirel. Propag. Lett.*, vol. 18, no. 10, pp. 2081–2085, Aug. 2019.

[7] G. Toso, P. Angeletti, and C. Mangenot, "A comparison of density and amplitude tapering for transmit active arrays," in *Proc. 3rd EuCAP*, Berlin, Germany, Mar. 2009.

[8] Y. Aslan, A. Roederer, and A. Yarovoy, "System advantages of using large-scale aperiodic array topologies in future mm-wave 5G/6G base stations: an interdisciplinary look," *IEEE Sys. J.*, 2021.

[9] T. Bai and R. W. Heath, "Coverage and rate analysis for millimeter-wave cellular networks," *IEEE Trans. Wireless Commun.*, vol. 14, no. 2, pp. 1100–1114, 2014.

[10] A. Thornburg, T. Bai, and R. W. Heath, "Performance analysis of outdoor mmwave ad hoc networks," *IEEE Trans. Signal Process.*, vol. 64, no. 15, pp. 4065–4079, 2016.

[11] X. Yu, J. Zhang, M. Haenggi, and K. B. Letaief, "Coverage analysis for millimeter wave networks: the impact of directional antenna arrays," *IEEE J. Sel. Areas Commun.*, vol. 35, no. 7, pp. 1498–1512, 2017.

[12] Z. Marzi and U. Madhow, "Interference management and capacity analysis for mm-wave picocells in urban canyons," *IEEE J. Sel. Areas Commun.*, vol. 37, no. 12, pp. 2715–2726, 2019.

[13] R. Wang *et al.*, "Stationarity region of mm-wave channel based on outdoor microcellular measurements at 28 GHz," in *Proc. IEEE MILCOM*, Baltimore, MD, USA, 2017, pp. 782–787.

[14] H. Zhao *et al.*, "28 GHz millimeter wave cellular communication measurements for reflection and penetration loss in and around buildings in New York city," in *Proc. IEEE ICC*, Budapest, Hungary, 2013, pp. 5163–5167.

[15] T. S. Rappaport, G. R. MacCartney, S. Sun, H. Yan, and S. Deng, "Small-scale, local area, and transitional millimeter wave propagation for 5G communications," *IEEE Trans. Antennas Propag.*, vol. 65, no. 12, pp. 6474–6490, 2017.

[16] Y. Aslan, J. Puskely, A. Roederer, and A. Yarovoy, "Performance comparison of single-and multi-lobe antenna arrays in 5G urban outdoor environments at mm-waves via intelligent ray tracing," in *Proc. 14th EuCAP*, Copenhagen, Denmark, 2020, pp. 1–5.

[17] E. V. Anjos *et al.*, "FORMAT: a reconfigurable tile-based antenna array system for 5G and 6G millimeter-wave testbeds," *IEEE Sys. J.*, 2022.

[18] Y. Aslan, "Optimization of virtually aperiodic linear sparse arrays," *Microw. Opt. Technol. Lett.*, vol. 64, no. 2, pp. 318–324, 2022.

[19] R. L. Haupt, "Adaptively thinned arrays," *IEEE Trans. Antennas Propag.*, vol. 63, no. 4, pp. 1626–1632, 2015.

[20] Y. Aslan, J. Puskely, A. Roederer, and A. Yarovoy, "Multiple beam synthesis of passively cooled 5G planar arrays using convex optimization," *IEEE Trans. Antennas Propag.*, vol. 68, no. 5, pp. 3557–3566, May 2020.

[21] B. Fuchs, A. Skrivervik, and J. R. Mosig, "Synthesis of uniform amplitude focused beam arrays," *IEEE Antennas Wireless Propag. Lett.*, vol. 11, pp. 1178–1181, Oct. 2012.

[22] L. Bui, N. Anselmi, T. Isernia, P. Rocca, and A. Morabito, "On bandwidth maximization of fixed-geometry arrays through convex programming," *J. Electromagnet. Wave.*, vol. 34, no. 5, pp. 581–600, 2020.

[23] H. B. Van, S. N. Jha, and C. Craeye, "Fast full-wave synthesis of printed antenna arrays including mutual coupling," *IEEE Trans. Antennas Propag.*, vol. 64, no. 12, pp. 5163–5171, Dec. 2016.

[24] T. Marinović *et al.*, "Fast characterization of mutually coupled array antennas using isolated antenna far-field data," *IEEE Trans. Antennas Propag.*, vol. 69, no. 1, pp. 206–218, 2020.

[25] M. Lobo, L. Vandenberghe, S. Boyd, and H. Lebret, "Applications of second-order cone programming," *Lin. Algebra Appl.*, vol. 284, no. 1–3, pp. 193–228, 1998.

[26] M. Grant and S. Boyd, "CVX: Matlab software for disciplined convex programming, version 2.1," http://cvxr.com/cvx, Mar. 2014.